energies

MDPI

Article

Automatic Adaptation of Multi-Loop Wireless Power Transfer to Variable Coupling between Transmit and Receive Coils

Kyeongmok Ryu and Jinho Jeong *

Department of Electronic Engineering, Sogang University, Seoul 04107, Korea; kyoungmok777@naver.com
* Correspondence: jjeong@sogang.ac.kr; Tel.: +82-2-705-8934

Received: 19 June 2018; Accepted: 5 July 2018; Published: 7 July 2018

Abstract: In the conventional wireless power transfer (WPT) using magnetic resonance coupling, power transfer efficiency (PTE) exhibits a peak only at a matched distance between transmitter (Tx) and receiver (Rx). That is, it rapidly degrades if the distance deviates from the matched distance. In order to achieve high PTE over a wide range of the distance, automatic range-adaptation technique is proposed in this work by using multi-loop technique and tunable matching circuit with digital capacitors. For automatic range adaptation, the microcontroller unit (MCU) in Rx runs an algorithm to find optimum loop and capacitance for best PTE based on the received power. Tx and Rx are synchronized by using low power Bluetooth wireless communications. Instead of the conventional relays, microelectromechanical system (MEMS) switches with low loss and high isolation are employed to minimize the power dissipation. The entire WPT system automatically maximize PTE with the distance, achieving high PTE of 80.5% at 30 cm and 29.7% at 100 cm.

Keywords: wireless power transfer (WPT); magnetic resonance; tunable impedance matching; range adaptation

1. Introduction

Magnetic resonant coupling technique allows an efficient wireless power transfer (WPT) up to a few meters, which can overcome the problem of the limited operating range of the magnetic induction technique. Therefore, it finds a lot of applications in the mid-range wireless charging of home appliances and electric vehicles. However, the efficiency peaks only at a specific distance between transmitter (Tx) and receiver (Rx), and it rapidly drops as the distance changes. Therefore, there are intensive researches to achieve the high efficiency even though the distance changes, what is called, range-adaptive WPTs, using frequency and impedance tuning techniques [1–8].

In the frequency tuning method, operating frequency is adjusted to provide low reflection and thus high efficiency depending on the distance or to overcome the frequency splitting effect at very near distance [1–4]. However, it needs a wide bandwidth of operation and frequency-tunable signal source. Impedance tuning technique is commonly used for range-adaptive WPTs. It is based on the fact that input impedance of magnetic resonant WPT is matched to the system impedance only at a specific distance and varies according to the distance. Therefore, the efficiency can be recovered if tunable matching circuit is utilized to match input impedance to system impedance depending on the distance. In [9–12], tunable capacitors, switching capacitors, and switches were used as tunable matching circuit (TMC) for the range-adaptive WPTs.

However, the input impedance of magnetic resonant WPTs exhibits very wide variation according to the distance. Therefore, the impedance tuning method alone can allow the very limited performance in the range adaption. In order to extend the adaptation range, the coupling between loop and coil can

be adjusted according to the distance by changing the orientation or the distance between loop and coil [5]. However, this method requires a mechanical tuning using motors for automatic adaptation which leads to the increase of DC power consumption and system complexity. Recently, multi-loop WPT has been introduced to improve the range adaptation [13] by the authors' group of this paper, where four loops with different size were employed, and only one loop was selected according to the distance. It adjusts the coupling factor between the coil and loop such that the variation of input impedance with distance is dramatically reduced. It allows the WPT to adapt and maintain high efficiency over wider range of the distance using simple TMC.

However, the multi-loop WPT in [13] employed three relays for the loop switching among four loops at each Tx and Rx. Even though relays provide very low loss, they have several drawbacks such as high power dissipation and low switching speed. In addition, input impedance was measured using directional coupler and rectifier which are also bulky and expensive. Moreover, a personal computer was used and connected to both Tx and Rx to calculate input impedance and to control the loop-switching and TMC. Thus, the WPT in [13] was not practical for real applications.

In this work, we propose an automatic range-adaptive WPT which is compact and low-power consuming, using microcontroller unit (MCU), MEMS switch, digital capacitors, and Bluetooth module. Therefore, it is well-suited for the practical applications. In the proposed WPT, MCU measures the received power at Rx and runs the algorithm to find the optimum loop and capacitances for impedance matching, so that the complex impedance measurement circuits and personal computer can be removed. The same loop and capacitance as those in Rx are selected in Tx via Bluetooth Low Energy (BLE) communications. In addition, MEMS SP4T switch allows low-loss and fast loop switching with almost no power consumption, compared with conventional relay switches. The varactor in the TMC is replaced with digital capacitors which can be easily controlled by digital signals of MCU. In Section 2, the details of the proposed system are explained together with the design considerations. The measured performance is presented in Section 3.

2. Proposed WPT System

2.1. System Operation

Figure 1 shows the block diagram of the proposed WPT system in this work, where four loops and single coil were used at the respective Tx and Rx. The operation frequency f_0 was 13.56 MHz. The loops had different diameters, and thus different mutual inductance with coil. During the operation, one of four loops was connected by the SP4T switch, and the impedance was matched by TMC, to provide the best efficiency with the distance between Tx and Rx. All of these procedures were automatically controlled by the MCUs, which are placed in both Tx and Rx. The MCU in Rx sets up wireless connection between the central and peripheral BLE modules to communicate the information on control voltages of the switches and TMCs. Then, both MCUs connect one of the loops (the same loop in Rx and Tx) and tune the TMC (the same value in Rx and Tx), and the Rx MCU measures the rectified voltage and computes efficiency. Finally, the Rx MCU finds and sets the optimum loop and TMC that generate maximum efficiency.

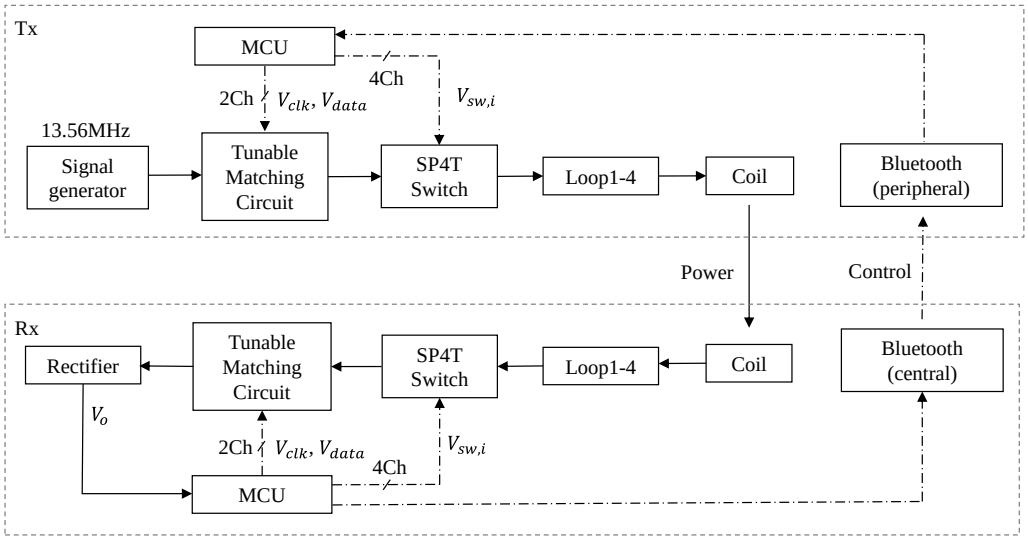

Figure 1. Block diagram of the proposed wireless power transfer (WPT) system.

Figure 2 shows the analog circuit part of the proposed WPT system which consists of a coil and four loops at Tx and Rx, respectively. As shown in this figure, Tx and Rx were symmetric except for the rectifier in Rx. That is, the coils, loops, series loop capacitors ($C_{l,i}$), SP4T switches, and TMCs (digital capacitor banks) were identical in Tx and Rx. Note that one of the four loops was only connected by an SP4T switch during the operation. TMC was simply designed using a shunt capacitance (digital capacitor bank) by modifying the loop capacitances from the resonant values. It will be explained later in more detail.

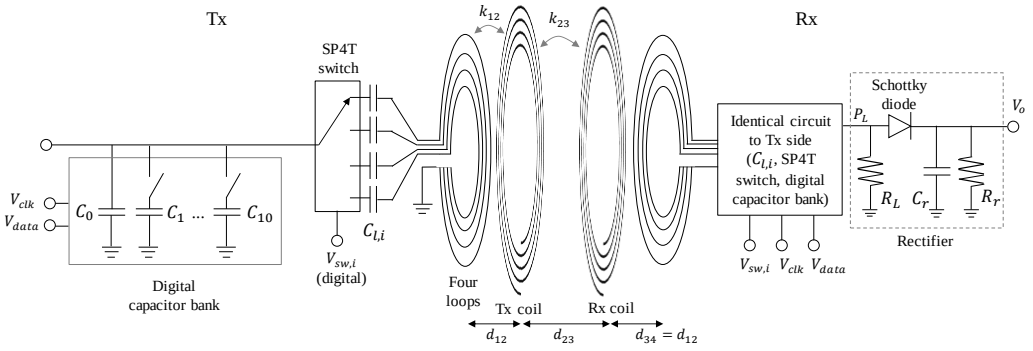

Figure 2. Analog circuit part of the proposed WPT system.

Prior to discussing multi-loop technique, a conventional wireless power transfer system using a single loop was analyzed using an equivalent circuit given in Figure 3. Coils are represented with self-inductance L_c, self-capacitance C_c, and resistance R_c. They were designed to resonate at f_0 and to provide high quality (Q) factor. A single-turn loop is represented with L_l and R_l. C_l is an external capacitor including a self-capacitance of the loop and determined to resonate with L_l at f_0. k_{12} and k_{23} are the coupling coefficients between coil and loop and between Tx and Rx coils, respectively. Power transfer efficiency (PTE) η and input impedance (Z_{in}) of the magnetic resonant WPT at f_0 are given by (1) and (2), respectively [5]:

$$\eta = \frac{P_L}{P_{avs}} = \left[\frac{2k_{23}k_{12}^2 Q_1 Q_2^2}{\left(1 + k_{12}^2 Q_1 Q_2\right)^2 + k_{23}^2 Q_2^2} \right]^2, \quad (1)$$

$$Z_{in} = R_0 \frac{Q_1 Q_2 k_{12}^2 (Q_1 Q_2 k_{12}^2 + 1)}{Q_2^2 k_{23}^2 + Q_1 Q_2 k_{12}^2 + 1} \quad (2)$$

where Q_1 and Q_2 are Q-factors of loop and coil at f_0, respectively. P_{avs} and P_L are the available power from Tx signal generator with source resistance R_0 (50 Ω), and the power delivered to the matched load (R_0) in Rx, respectively. Therefore, the PTE η in (1) is equal to transducer power gain ($|S_{21}|^2$) of the 2-port network shown in Figure 3a with reference impedance R_0 [13,14]. In this paper, the term PTE or efficiency is used to evaluate the performance of the wireless power transfer system. Note that k_{23} is proportional to $1/d_{23}^3$, where d_{23} is the distance between the coils in Tx and Rx [14,15]. From (1), it can be found that PTE is a strong function of the distance, d_{23}, and there exists an optimum $k_{23,opt}$ or $d_{23,opt}$ given by (3), providing a maximum PTE, at which the input impedance (Z_{in}) is matched to R_0 (system reference impedance):

$$k_{23,opt} = \sqrt{k_{12}^4 Q_1^2 - 1/Q_2^2} \quad (3)$$

Figure 3b shows the simulated PTE using the parameters of the loop and coil fabricated in this work which are given in Tables 1 and 2. The loop 1 was used in this simulation with a capacitance C_l of 120.7 pF resonating with L_l = 1.141 μH at f_0 = 13.56 MHz. As shown in this figure, the conventional WPT system with a single loop (loop 1) showed a very high PTE of 87.0% at d_{23} = 32.5 cm which was an optimum distance ($d_{23,opt}$) in this case. However, PTE rapidly decreased if d_{23} deviated from 32.5 cm.

Figure 4 shows the simulated Re $\{Z_{in}\}$ and Im $\{Z_{in}\}$ as a function of the distance d_{23} of the conventional WPT system (a). It is shown in this figure that Z_{in} was matched to R_0 at $d_{23} = d_{23,opt}$ = 32.5 cm, and varied with the distance, as also implied by (1) and (2). Therefore, in order to achieve high PTE, TMC can be designed such that Z_{in} should be matched to R_0 as d_{23} changes. However, the conventional single-loop WPT showed very wide variation in Z_{in} as d_{23} changed from 10 to 100 cm; real part from 4.5 to 760.4 Ω, and the imaginary part from 0.0 to −j85.6 Ω. Therefore, complex TMC is required to transform widely-varying Z_{in} to R_0 [9–11].

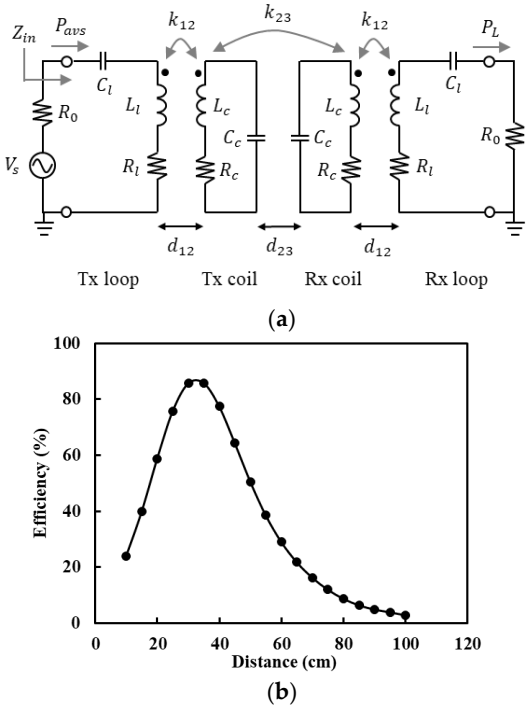

Figure 3. A conventional single-loop WPT system: (**a**) Equivalent circuit; (**b**) Simulated efficiency with the distance (d_{23}).

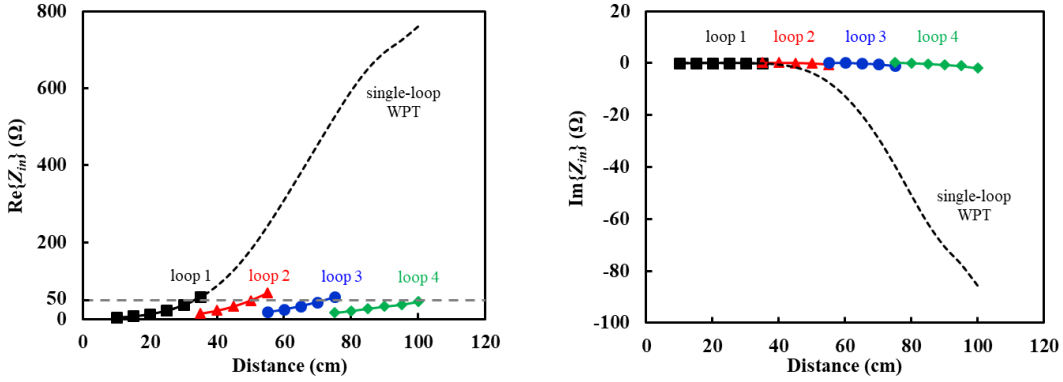

Figure 4. Simulated input impedance Z_{in} of WPT system with the distance: (**a**) real part; (**b**) imaginary part.

In order to solve this problem, the multi-loop WPT can be used based on the fact that $k_{23,opt}$ or $d_{23,opt}$ is a function of k_{12} from (3) [13]. The coupling factor k_{12} between loop and coil can be adjusted by changing the distance d_{12} or the size of the loop. In the multi-loop WPT, k_{12} was adjusted by connecting a different size loop depending on d_{23}, so that there could exist several optimum distances providing impedance matches. In addition, connecting one of four loops depending on the distance greatly reduced Z_{in} variation as shown in Figure 4, where Re $\{Z_{in}\}$ and Im $\{Z_{in}\}$ varied from 4.5 to 67.5 Ω, and from 0.2 to −1.9 Ω, respectively, while d_{23} changed from 10 to 100 cm. Therefore, the combination of the multi-loop technique and tunable matching can maintain high PTE over a wide range of the distance. Z_{in} also varies as the load impedance changes. The simulation shows that this variation due to the load impedance can be mitigated by using multiple loops instead of a single loop.

2.2. Tunable Matching Circuit

As stated earlier, the multi-loop technique can greatly reduce the Z_{in} variation with respect to d_{23}, which simplifies TMC design. In the conventional single-loop WPT system, the loop capacitance C_l was determined to resonate at f_0 with the loop inductance L_l. In this work, we used higher loop capacitance ($C_{l,i}$) (as listed in Table 3) so that input impedance became inductive, as shown in Figure 5, and thus impedance match could be simply fulfilled by using a single shunt capacitor only. Figure 5 shows the input impedance of the WPT system on a Smith chart at distances 40, 45, and 50 cm when the loop 2 is selected. As illustrated, a simple shunt capacitor (173, 120, and 55 pF, respectively) is enough to transform input impedances to R_0.

A tunable capacitor can be implemented by varactor or digital capacitor bank. The varactor exhibits a relatively small capacitance variation ratio (<1:3.25) considering power handling capability and breakdown and requires an analog control voltage, which is generated by low-pass filtering the PWM output of the MCU [13]. The low-pass filter should be designed to have enough settling time to reduce the ripples in the control voltages, which leads to a long time required to tune the capacitance.

On the contrary, the digital capacitor bank can be easily tuned at very high speed by the MCU. In this work, five of 10-bit digital capacitors (NCD2100TTR by IXYS) were used in parallel as tunable capacitors to provide the capacitance from 33.0–187.8 pF (1:5.69), depending on the digital control voltages, as illustrated in Figure 2. The capacitance was adjusted to a very high speed of 220 μsec by applying a serial digital data (V_{data}) and clock signal (V_{clk}) from MCU.

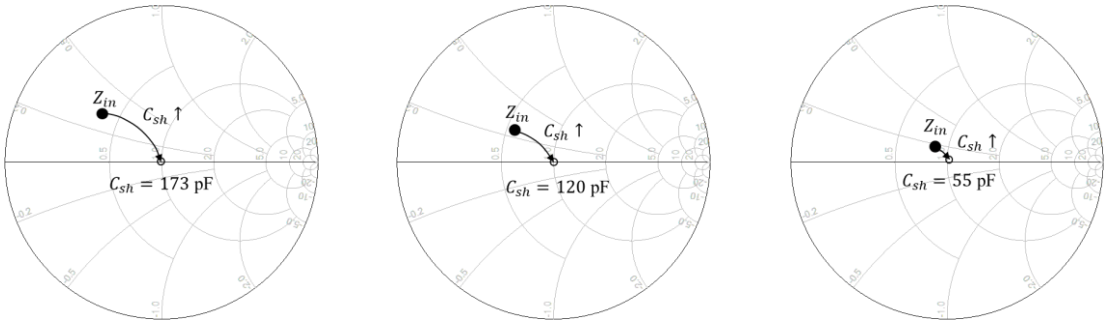

(a) (b) (c)

Figure 5. Impedance matching using a shunt capacitor (C_{sh}) at distances of (**a**) 40, (**b**) 45, and (**c**) 50 cm with the loop 2 selected.

2.3. Coil and Loops

The number of turns and diameter of the coil were determined to provide a high *Q*-factor at the resonance frequency f_0 of 13.56 MHz. There were four loops with different sizes, as shown in Figure 2. The diameter of each loop was determined such that the coupling coefficient (k_{12}) between the coil and the loop allowed impedance match at certain distances. For example, the largest loop 1 (diameter = 34 cm) allowed an impedance match at around d_{23} = 35 cm, and the smallest loop 4 around d_{23} = 100 cm. Therefore, one of the four loops will be connected by the SP4T switch to provide an impedance match depending on the distance d_{23}. The coils and loops were fabricated using a copper wire of a diameter of 0.3 cm and their dimensions are presented in Table 1. This includes the extracted inductance, *Q*-factor, and resistance from the measured data using vector network analyzer and LCR meter.

The coil and loops were separated by 1.5 cm (d_{12}). Coupling coefficients k_{12} between the coil and each loop were computed using INCA calculator and listed in Table 1 [16]. The same tool was also used to find coupling coefficients k_{23} between Tx and Rx coils as a function of distance d_{23} as listed in Table 2. The values in Tables 1 and 2 were used to design and simulate the conventional single-loop and proposed multi-loop WPT systems.

Table 1. Fabricated coils and loops.

Parameter	Tx coil	Rx coil	Loop 1	Loop 2	Loop 3	Loop 4
Number of turns	4	4	1	1	1	1
Diameter (cm)	68.0	68.0	34.0	29.0	24.5	20.5
Inductance (μH)	15.344	15.244	1.141	0.955	0.786	0.610
Resistance (Ω)	7.713	7.844	0.67	0.50	0.36	0.28
Q-factor at f_0	169.438	165.519	145.5	162.1	184.0	188.3
k_{12}	-	-	0.232	0.175	0.133	0.101

Table 2. Computed coupling coefficients (k_{23}) with the distance (d_{23}).

d_{23} (cm)	10	20	30	40	50	60	70	80	90	100
k_{23}	0.3858	0.2090	0.1236	0.07745	0.05082	0.03467	0.02448	0.01780	0.01328	0.01013

Table 3. Values of loop capacitors and rectifier.

$C_{l,1}$ (pF)	$C_{l,2}$ (pF)	$C_{l,3}$ (pF)	$C_{l,4}$ (pF)	R_L (Ω)	R_r (MΩ)	C_r (nF)
160	200	260	270	50	10	100

2.4. SP4T Switch

In the proposed WPT, one of four loops was connected depending on the distance, which was carried out by the SP4T switch. Relays (ARE10A06 by Panasonic) are widely used as switches, since they have high power capability, very low loss (~0 dB), and high isolation at a few tens of MHz frequencies [13]. However, they consume a lot of direct current (DC) power (200 mW per relay) with low switching speed (~10 ms). In addition, the driver circuit was required, because MCU output current is too small to directly drive the relays. In order to solve these problems, the relays can be replaced with semiconductor switches, which have almost no DC power consumption, high switching speed, and simple driver circuit. However, the semiconductor switch exhibits a non-negligible loss even at a few tens of MHz frequencies. For example, the GaAs SPDT switch (HMC544A by Analog Devices) shows 0.25 dB loss at f_0 (13.56 MHz), so that total loss of the SP4T switch is 0.5 dB. It corresponds to an on-resistance of 5.3 Ω. This may drastically reduce PTE of the WPT system, when the input impedance of the WPT system (Z_{in} in Figure 3a) is lower than 50 Ω. In the WPT system in [13], Re $\{Z_{in}\}$ ranges from 5 to 50 Ω and is matched to 50 Ω by TMC. Figure 6 shows the simulated loss of the switch with on-resistance of 5.3 Ω when the switch is terminated with the impedance Z_{term} at both ports. The loss is 0.5 dB (efficiency = 89.1%) at Z_{term} = 50 Ω. It greatly increases to 3.7 dB (efficiency = 42.6%) at Z_{term} = 5 Ω. Note that the switch is used at both Tx and Rx, so that the total PTE will be dramatically reduced by the loss of the switch. Therefore, the semiconductor switches are not well-suited for high PTE WPT systems.

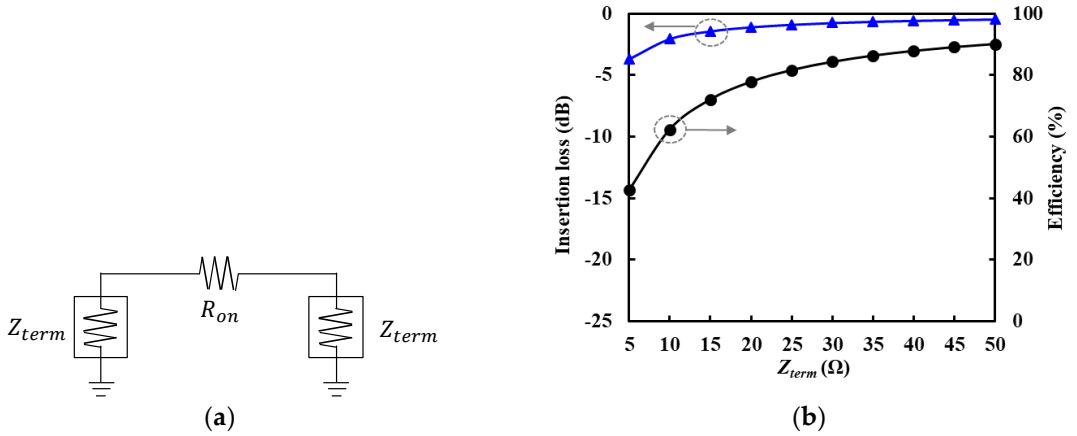

Figure 6. Simulation of the switch loss as a function of termination resistance Z_{term}: (**a**) Circuit simulation setup; (**b**) Insertion loss and power transfer efficiency (PTE) of the switch with on-resistance (R_{on}) of 5.3 Ω as a function of Z_{term}.

In order to minimize the PTE degradation due to the switch, we adopted a very low-loss SP4T MEMS switch (ADGM1304EBZ by Analog Devices). It exhibits about 0.12 dB loss at 13.56 MHz (on-resistance of 1.6 Ω) which allows only 1.3 dB loss even at Z_{term} = 5 Ω. It also allowed high switching speed (~30 μs) and low power dissipation of 9.9 mW, which was consumed by a companion driver integrated circuit (IC) to generate the high drive voltage of the MEMS switch. In addition, it operated as reflective open at off ports and has very high isolation about 70 dB, which were essential to minimizing the energy coupling to the unselected loops. The digital outputs of the MCU directly controlled the MEMS switch and selected one of four ports to be connected.

2.5. Rectifier

As shown in Figure 2, the Rx was terminated with a matched load R_L of 50 Ω. The power transferred to the matched load was converted to DC voltage (V_o) by the rectifier, which was connected in parallel with a load R_L. The rectifier exhibited a very high input impedance at 13.56 MHz, so that

it did not change the Rx termination impedance. The designed rectifier consisted of Schottky diode (SMS7621 by Skyworks) and RC filter (C_r and R_r in Table 3) minimizing the ripples in V_o. DC output voltage (V_o) is proportional to input power (P_L) or the received power. Therefore, the measured V_o was used to estimate the received power and find the optimum loop and capacitance for best efficiency. It was read by the MCU with 10-bit analog-to-digital converter (ADC), which allowed the voltage resolution of 3.22 mV, which corresponds to PTE uncertainty less than 1%. Figure 7 shows the measured relation between P_L and V_o with a fitted-curve, where P_L is an input power to a load R_L with the rectifier in parallel as shown in Figure 2. The Rx MCU utilizes the fitted polynomial equation (4) to calculate the received power P_L from the read V_o and compute PTE:

$$P_L = -25.5253{V_o}^4 + 78.4156{V_o}^3 - 95.3105{V_o}^2 + 64.3556V_o - 10.9397 \quad (4)$$

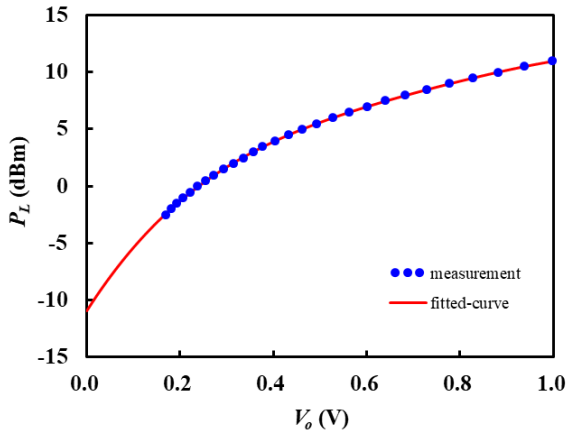

Figure 7. Measured and fitted relation between input power (P_L in dBm) and output voltage (V_o in V) of the rectifier.

2.6. MCU and BLE Module

MCU performs searching and setting the optimum loop and capacitance for the best PTE based on the measured V_o. For this purpose, we selected a low power MCU (Arduino promini) operating at 3.3 V with current consumption of 2 mA. The BLE module (FBL780BC by Firmtech) allowed wireless connection between Tx and Rx with a low power consumption (6.6 mW).

For automatic range-adaptation, the fast algorithm was developed as shown below to effectively find the optimum loop and capacitor control voltages. At first, the Rx MCU and the BLE modules would find and start communication with Tx BLE module. Then, the Rx MCU would order the Tx MCU to start the following searching algorithm such that Rx and Tx would simultaneously perform the loop selection and capacitance control.

1. Both Rx and Tx connect the loop 1 ($V_{sw,i}$ = 3.3 V for i = 1 and 0 V for otherwise).
2. For a selected loop, both Rx and Tx change the capacitance from low to high values at 8 points, and Rx MCU measure the rectified voltage V_o at each capacitance.
3. The procedure 2 is repeated for the loop 2, 3, and 4.
4. Rx MCU determines the optimum loop and capacitance, providing highest V_o and η, and send this information to Tx MCU through BLE.
5. Both Rx and Tx set the optimum loop and capacitance determined in the procedure 4.
6. Rx MCU measures V_o and calculates η periodically (every one second). If η is 5% less than η_{max}, select the loop 1 and repeat the process from the procedure 2.

3. Experimental Results

Figure 8a shows the fabricated WPT system for the experiment. Coils and loops were fixed on acrylic plates. A signal generator (Rhode & Schwarz SML 03) is used as a power source producing 10-dBm CW power at 13.56 MHz. It was connected to the input port of Tx circuit. Detailed views of Tx and Rx circuits are shown in Figure 8b,c. For this proof-of-concept experiment, the evaluation board of the SP4T MEMS switch was utilized, and digital capacitors were soldered onto the sockets. Available power (P_{avs}) from the signal generator was measured by a power meter (Agilent E4417A) and the delivered power to Rx (P_L) was computed from the measured rectifier output voltage using (4). Then, the efficiency was calculated using (1). The efficiency calculation was confirmed by *S*-parameter measurement of the system (Figure 2) without the rectifier using vector network analyzer. Note that DC power consumption of the MCU and BLE modules, and the MEMS switch, was not included in the efficiency calculation.

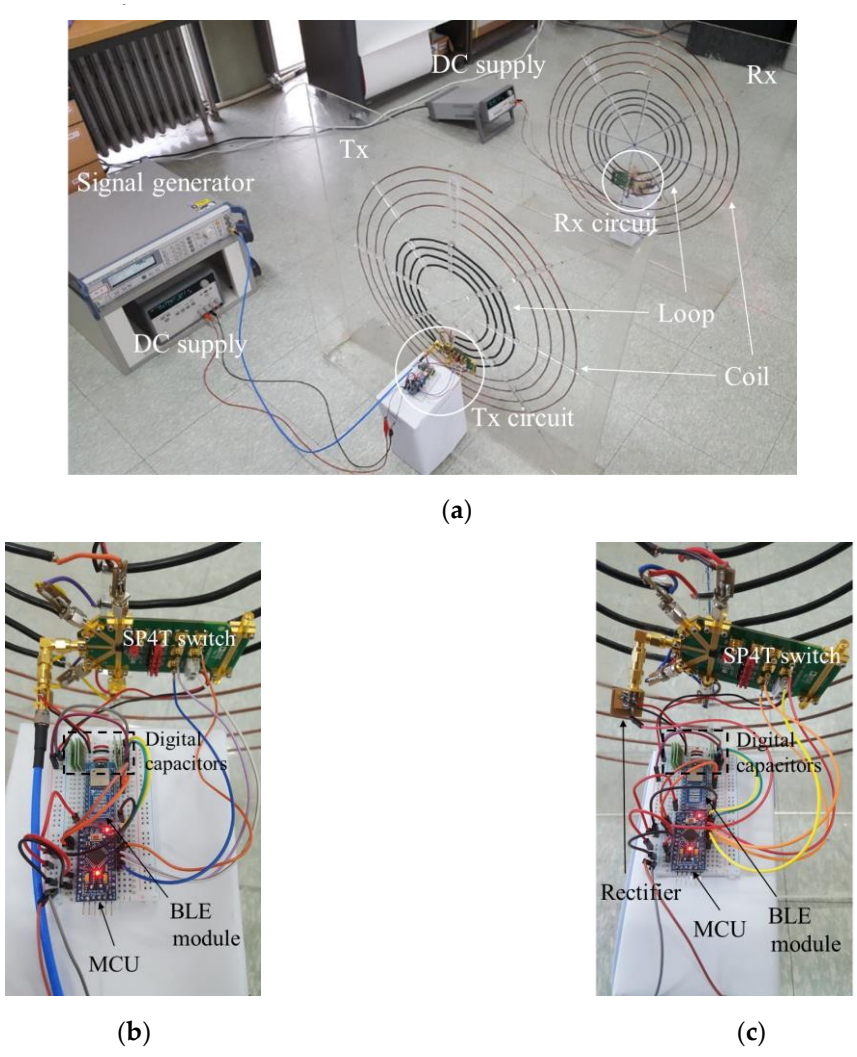

Figure 8. Photograph of the fabricated system: (**a**) Entire system; (**b**) Tx circuit; (**c**) Rx circuit.

At first, Tx and Rx coils were separated by 50 cm and then Rx MCU performed to find the optimum loop and capacitance following the procedure explained in Section 2.6. After the loop was selected from 1 to 4, the capacitance was digitally controlled from 33.0–187.8 pF at an increment of 22.1 pF (or 8 steps). More fine tuning of the capacitance (16 steps) can lead to a little higher optimum efficiency (~0.1%) at the cost of a longer searching time. Figure 9 shows the measured efficiency at

every loop and capacitance combination as a function of an elapsed time. Based on this experiment, the loop 2 was selected and the capacitance was set to 33.0 pF to achieve a maximum efficiency of 71.2% at d_{23} = 50 cm. Total searching time was just 320 msec. There were a total 32 combinations of loop and capacitance. Each combination took 10 msec for the measurement, including 220 µsec for capacitance setting, 5 msec delay for Tx/Rx synchronization, and eight rounds of reading and averaging of the rectifier output voltages. After the search was finished, another 20 msec was taken to determine and set the optimum loop and capacitance in both Tx and Rx. Thus, total time required was only 340 msec to find and set the WPT systems to operate at highest efficiency. Total DC power consumption by MCU and BLE module was only 13.2 mW under a 3.3 V supply. It can be further reduced by adopting more power-efficient components so that the proposed system can be more self-sustainable.

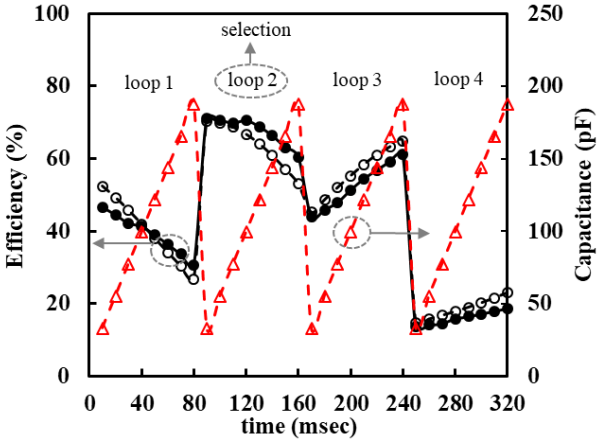

Figure 9. Measured and simulated efficiency at d_{23} = 50 cm as a function of time. The frequency was 13.56 MHz; solid lines with filled symbols: measurement, slotted lines with empty symbols: simulation.

Figure 10 shows the measured and simulated efficiency of the fabricated WPT system as a function of the distance d_{23}. Tx and Rx were manually separated from 10 to 100 cm in an increment of 5 cm. Note that the efficiency in this figure is a maximum value at a specific distance when optimum loop and capacitance were selected. This figure clearly shows that PTE exhibited a high value only in a narrow distance range if a single loop was used only with the impedance tuning technique. For example, when loop 1 was used only in WPT, the peak PTE was 80.5% at d_{23} = 30 cm, and it decreased to 41.6% at d_{23} = 50 cm. On contrast, in the multi-loop WPT, a loop 2 could be selected at d_{23} = 50 cm, achieving a much higher PTE of 73.2% which corresponded to a 31.6% point improvement. At a very long distance of 100 cm, the loop 4 was selected and the PTE was 29.7%. In short, the multi-loop technique could achieve high efficiencies over a wide range of distance. The simulation results were also included in Figure 10, showing a very good agreement with the measurement. The simulation was carried out by the commercial circuit simulator using the component values given in Tables 1–3.

At very near distances less than 20 cm, PTE rapidly dropped due to the frequency splitting effect [1,17]. That is, the resonant frequency started to separate into two frequencies at a tightly coupled transformer. In this case, PTE can be recovered by changing the frequency of the input signal. PTE was increased to 85.9% at 10 cm, with the input signal at 10.60 MHz instead of 13.56 MHz, as shown in Figure 10 (86.0% at 15 cm with input signal at 11.30 MHz, and 86.5% at 20 cm with input signal at 12.10 MHz).

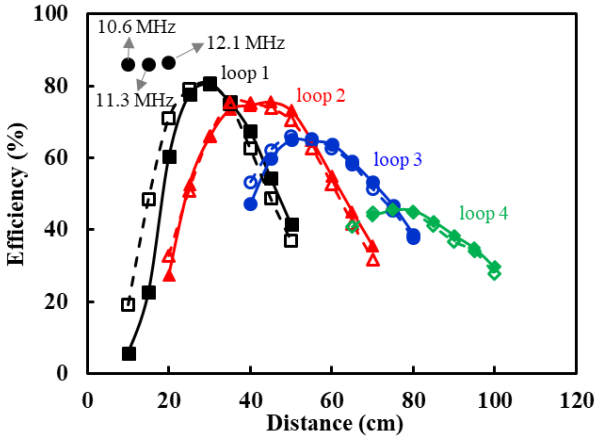

Figure 10. Measured and simulated PTE as a function of distance at 13.56 MHz unless otherwise specified; solid lines with filled symbols: measurement, slotted lines with empty symbols: simulation.

In the above experiment, the Tx and Rx coils were placed in parallel, that is, the angle between Tx and Rx coil planes is 0°. If Rx coil is rotated from 0°, the coupling coefficient (k_{23}) decreases and efficiency was degraded compared with Rx coil at 0°. Figure 11 shows the measured PTE when Rx coil was rotated by 30° at the distance d_{23} from 30 to 100 cm. The efficiency was a little bit degraded from the case with Rx coil at 0° at the same distance, because of the reduced coupling efficiency. However, this measurement result indicates that the system automatically tries to achieve high efficiency even though Tx and Rx coil are not in parallel.

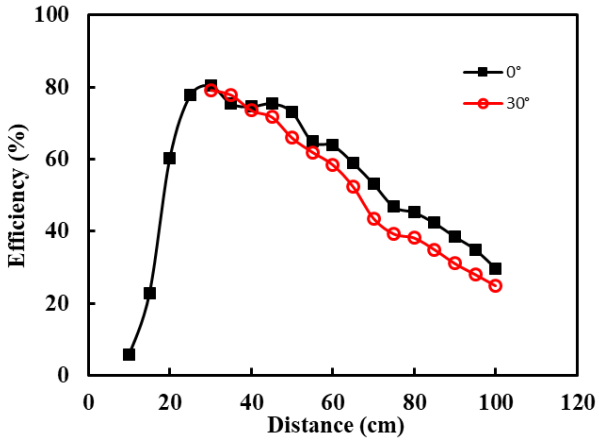

Figure 11. Measured PTE as a function of distance at 13.56 MHz depending on the angle of Tx and Rx coils. A 0° curve represent the efficiency in the case that Tx and Rx coils are in parallel.

4. Conclusions

In this paper, an automatic range-adaptation of magnetic resonant WPT was successfully accomplished over a wide range of the distance using multi-loop and digital capacitors. The whole process, searching and setting the optimum loop and tuning voltages at both Tx and Rx, was performed by using MCU and BLE modules. The proposed range-adaptive WPT system dissipates a very small DC power by replacing the relays with MEMS switch, and by using low power MCU and BLEs. In addition, a simple rectifier was utilized to compute the received power and efficiency, replacing bulky and expensive directional couplers. Therefore, the proposed WPT can be promising for the practical applications such as wireless charging of electrical devices and wireless sensors. For example, the Rx MCU can be used to connect sensors and actuators of which the power as well as of the MCU

itself will be supplied by the proposed WPT system. In this application, Bluetooth BLE plays a great role in wireless data communication between Tx and Rx, as well as for the control of Tx and Rx circuits, for high efficiency wireless power transfer.

Author Contributions: J. Jeong conceived and designed the experiments; K. Ryu performed the experiments; K. Ryu and J. Jeong analyzed the data; K. Ryu and J. Jeong wrote the paper.

Funding: This work was funded by the Korean Government (MSIT) (No.2018R1A2B2004098).

Acknowledgments: This work was supported by the National Research Foundation of Korea (NRF) grant funded by the Korea Government (MSIT) (No.2018R1A2B2004098).

Conflicts of Interest: The authors declare no conflict of interest.

References

1. Sample, A.P.; Meyer, D.T.; Smith, J.R. Analysis, experimental results, and range adaptation of magnetically coupled resonators for wireless power transfer. *IEEE Trans. Ind. Electron.* **2011**, *58*, 544–554. [CrossRef]
2. Si, P.; Hu, A.P.; Malpas, S.; Budgett, D. A frequency control method for regulating wireless power to implantable devices. *IEEE Trans. Biomed. Circuits Syst.* **2008**, *2*, 22–29. [CrossRef] [PubMed]
3. Park, J.; Tak, Y.; Kim, Y.; Kim, Y.; Nam, S. Investigation of adaptive matching methods for near-field wireless power transfer. *IEEE Trans. Antennas Propag.* **2011**, *59*, 1769–1773. [CrossRef]
4. Kim, N.Y.; Kim, K.Y.; Choi, J.; Kim, C.-W. Adaptive frequency with power-level tracking system for efficient magnetic resonance wireless power transfer. *Electorn. Lett.* **2012**, *48*, 452–454. [CrossRef]
5. Duong, T.P.; Lee, J.W. Experimental results of high-efficiency resonant coupling wireless power transfer using a variable coupling method. *IEEE Microw. Wireless Compon. Lett.* **2011**, *21*, 442–444. [CrossRef]
6. Waters, B.H.; Sample, A.P.; Bonde, P.; Smith, J.R. Powering a ventricular assist device (VAD) with the free-range resonant electrical energy. *Proceedings of the IEEE* **2012**, *100*, 138–149. [CrossRef]
7. Aldhaher, S.; Luk, P.C.-K.; Whidborne, J.F. Electronic tuning of misaligned coils in wireless power transfer systems. *IEEE Trans. Power Electorn.* **2014**, *29*, 5975–5982. [CrossRef]
8. Rozman, M.; Fernando, M.; Adebisi, B.; Rabie, K.M.; Kharel, R.; Ikpehai, A.; Gacanin, H. Combined Conformal Strongly-Coupled Magnetic Resonance for Efficient Wireless Power Transfer. *Energies* **2017**, *10*, 498. [CrossRef]
9. Beh, T.; Kato, M.; Imura, T.; Oh, S.; Hori, Y. Automated impedance matching system for robust wireless power transfer via magnetic resonance coupling. *IEEE Trans. Ind. Electron.* **2013**, *60*, 3689–3698. [CrossRef]
10. Waters, B.H.; Sample, A.P.; Smith, J.R. Adaptive impedance matching for magnetically coupled resonators. In Proceedings of the PIERS, Moscow, Russia, 19–23 August 2012; pp. 694–701.
11. Lim, Y.; Tang, H.; Lim, S.; Park, J. An adaptive impedance-matching network based on a novel capacitor matrix for wireless power transfer. *IEEE Trans. Power Electron.* **2014**, *29*, 4403–4413. [CrossRef]
12. Lee, W.; Lee, H.; Oh, K.; Yu, J. Switchable distance-based impedance matching networks for a tunable HF system. *Progr. Electromagn. Res.* **2012**, *128*, 19–34. [CrossRef]
13. Kim, J.; Jeong, J. Range-Adaptive Wireless Power Transfer Using Multiloop and Tunable Matching Techniques. *IEEE Trans. Ind. Electorn.* **2015**, *62*, 6233–6241. [CrossRef]
14. Kim, J.; Choi, W.; Jeong, J. Loop switching technique for wireless power transfer using magnetic resonance coupling. *Progr. Electromagn. Res.* **2013**, *138*, 197–209. [CrossRef]
15. Raju, S.; Wu, R.; Chan, M.; Yue, C.P. Modeling of Mutual Coupling between Planar Inductors in Wireless Power Applications. *IEEE Trans. Power Electorn.* **2014**, *29*, 481–490. [CrossRef]
16. Musznicki, P.; Mandrek, S.; Chrzan, P.J. Modelling of PCB layout parasitic for resonant DC link inverter. In Proceedings of the Summer Seminar on Nordic Network for Multi Disciplinary Optimised Electric Drives NorMUD, Gdansk-Jurata, Poland, 2–4 September 2005; pp. 71–74.
17. Zhang, Y.; Zhao, Z.; Chen, K. Frequency-Splitting Analysis of Four-Coil Resonant Wireless Power Transfer. *IEEE Trans. Ind. Appl.* **2014**, *50*, 2436–2445. [CrossRef]